Sensorless Control of High Power Induction Motors Using Multilevel Converters

K. Saleh, M. Sumner, G. Asher, Q. Gao
Department of Electrical and Electronic Engineering,
University of Nottingham, Nottingham, U.K.
eexks4@nottingham.ac.uk

Keywords: Induction motor, Multilevel converter, Sensorless control.

Abstract

This paper introduces a new scheme to track the rotor position of an induction motor, which reduces distortion introduced into the motor current by sensorless control techniques. The scheme uses the measurement of current derivatives in response to test vectors imposed during the null switching vectors of a standard PWM scheme. The test vectors are derived from H-Bridges connected in series with the main converter. These H-Bridges generate a lower voltage test vectors which will reduce the distortion in the motor current directly without compromising the quality of the sensorless performance of the system. The proposed application of this sensorless technique is to high power multilevel converters which use a combination of series connected GTO and IGBT based H bridges to achieve a reasonable quality medium voltage waveform for motor drives, although there are now similar topologies proposed for automotive drives. The implementation of this sensorless technique in such applications requires modification to the control software only.

1 Introduction

The estimation of the rotor position through tracking the variation of the motor leakage inductances has been reported in [1,2,3,4,5]. The motor leakage inductance varies due to geometric or saturation saliency, and is used as an indication of rotor or flux position. By measuring the dynamic response of the motor's stator currents (di/dt) in response to inverter switching actions, the position of the saliency can be tracked. These inverter switching actions can be either due to special test vectors such as those used by the INFORM method [1] or can be the normal PWM waveform as used in the fundamental PWM method [3]. The di/dt measurement can then be used to reconstruct a resolver like signal to track flux or rotor position.

When a new switching vector is imposed onto a motor by switching an IGBT, the switching action excites the parasitic capacitances within the inverter and motor and causes high frequency oscillations in the motor current. Parasitic capacitances to ground (e.g motor winding to case, IGBT to heatsink) cause common mode oscillations and inter phase capacitances (inter-turn in the motor) cause differential mode oscillations. These high frequency oscillations will last for few microseconds as shown in Fig 1. The correct current response can be only measured after these oscillations have died out. The time required for the oscillation to decay is called minimum pulse width (t_{min}).

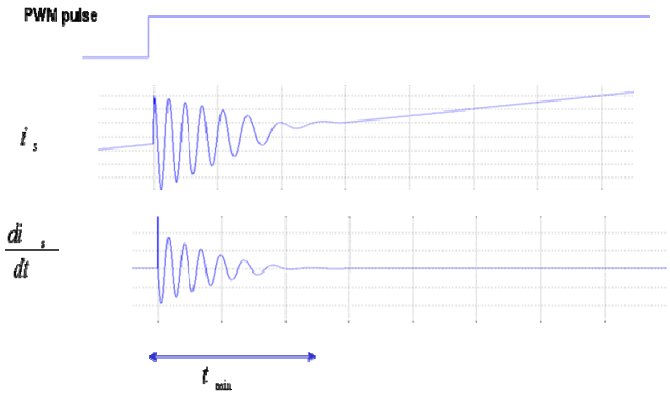

Fig 1:HF oscillations when IGBT switches state

The implementation of all pulse based or PWM based excitation methods introduces a minimum voltage vector pulse width (t_{min}) into the operation of the drive which introduces a large distortion in the motor currents at low speeds as show in Fig 2 and Fig 3 for the INFORM and the fundamental PWM methods respectively. This distortion causes audible noise, torque pulsation and increases losses.

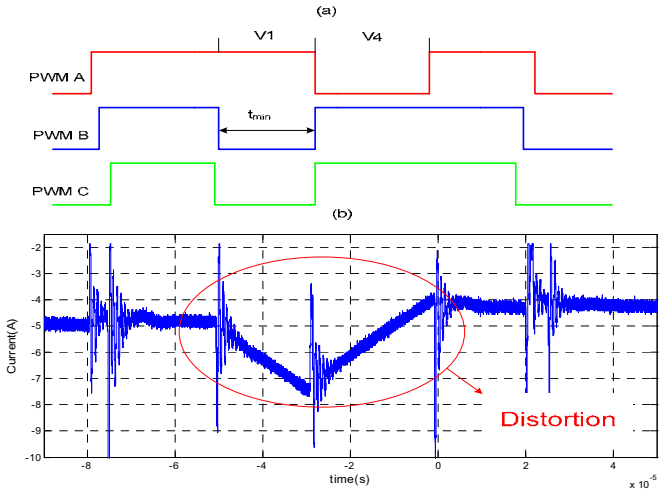

Fig 2: Current response in the fundamental PWM method (a) PWM waveform(b) dynamic current response

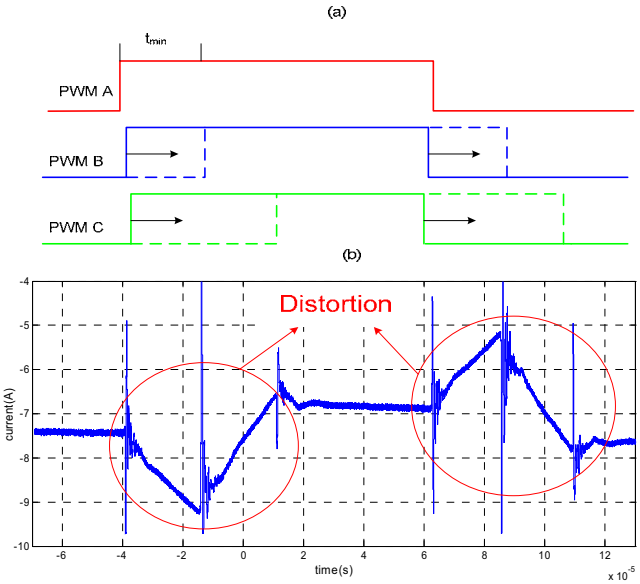

Fig 3:Dynamic current response in the INFORM method (a) PWM waveform (b) dynamic current response

A new scheme is proposed to track the rotor position of an induction motor in this paper. It uses the measurement of current derivatives in response to test vectors imposed during null switching vectors of a standard PWM scheme. The test vectors are imposed using H-Bridges connected in series with the main converter to generate test vectors during the null vector, in a similar way to that proposed in [14]. The test vectors have a lower voltage and this reduces the distortion in the current directly, as well as shortening the minimum pulse width (t_{min}) adding a further improvement to current distortion without compromising the quality of the sensorless performance of the system. It is the improvement in the motor current waveform that is specifically described in this paper, compared to [14], which concentrates on the sensorless performance. The proposed application of this sensorless technique is to high power multilevel converters which use a combination of series connected GTO and IGBT based H bridges to achieve a reasonable quality medium voltage waveform for motor drives, although there are now similar topologies proposed for automotive drives. The implementation of this sensorless technique in such applications requires modification to the control software only.

3 The addition of H-Bridges for test pulses

Fig 4 shows the schematic for the multilevel converter developed for this project [6,7]. Three H Bridges have been connected to a standard inverter. This configuration is designed to evaluate the principle of the method even if it does not use the envisaged target topology. It is however anticipated that the method developed here will be applicable to very high power induction motor drives fed from "isolated cell" multi-level converters which employ different switching devices and cell voltages as proposed in [8,9]

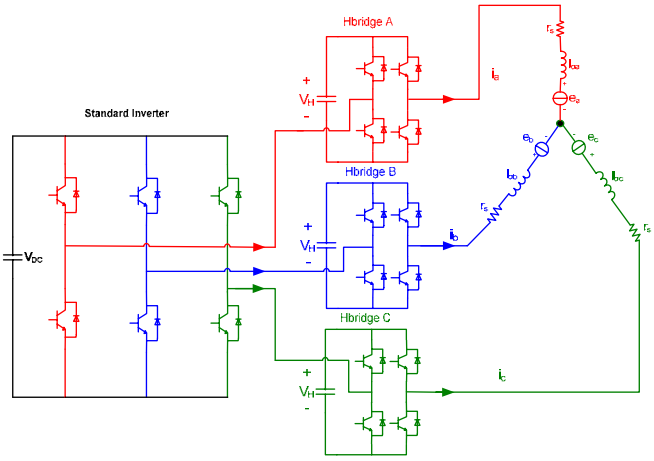

Fig 4: Topology of the prototype multilevel converter .

During normal operation, no additional test-pulses are imposed on the machine, and the H-Bridges will have a switching pattern that produces zero volts at their outputs as shown in Fig 5.a i.e. the upper two IGBTs will be ON. When a positive pulse ($+V_H$) is required from a particular H Bridge, to impose a positive "test pulse" on that machine phase winding, the switching pattern of the H-Bridge will be as shown in Fig 5.b. Finally when a negative test-pulse ($-V_H$) is required, the H-Bridge will have a switching pattern as seen in Fig 5.c.

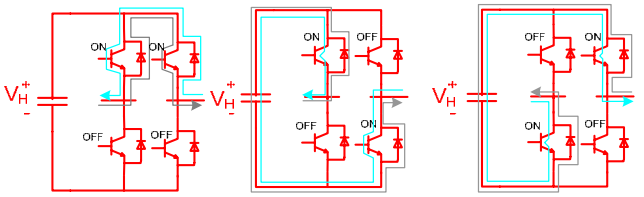

Fig 5.a: H-Bridge switching and current directions to produce 0 V output voltage

Fig 5.b: H-Bridge switching and current directions to produce $+V_H$ V output voltage

Fig 5.c: H-Bridge switching and current directions to produce $-V_H$ V output voltage

4 Tracking the Rotor Slotting Saliency

The stator leakage inductances of the induction motor are modulated by anisotropy either from the rotor slotting or from the saturation of the main flux. The modulation can be expressed by the following equations:-

$$l\sigma a = L_0 + \Delta L cos(n_{an}\theta_{an}) \quad (1)$$

$$l\sigma b = L_0 + \Delta L cos\left(n_{an}(\theta_{an} - \frac{2\pi}{3}\right) \quad (2)$$

$$l\sigma c = L_0 + \Delta L cos\left(n_{an}(\theta_{an} - \frac{4\pi}{3}\right) \quad (3)$$

Where L_0 is the average inductance and ΔL is the variation of leakage inductance due to the rotor anisotropy (n_{an}=2 for saturation anisotropy , and $n_{an} = \frac{N_r}{p}$ for rotor slotting , where N_r is the rotor slot number and p is the number of pole pairs).

The modulation of the stator leakage inductances can be seen in the transient response of the motor line current to the test

vectors imposed by the H-Bridges shown in Fig 6. By measuring the transient current (di/dt) in response to the test vector it is possible to detect the inductance variation and track the rotor position. This is derived as follows.

When H-Bridge A imposes the $+V_H$ test pulse the following equations can be derived using the machine equivalent circuit shown in Fig 4 :-

$$+V_H = \overbrace{r_s i_a + l_{\sigma a}\frac{di_a}{dt} + e_a - r_s i_b - l_{\sigma b}\frac{di_b}{dt} - e_b}^{(+V_H)} \quad (4)$$

$$0 = \overbrace{r_s i_b + l_{\sigma b}\frac{di_b}{dt} + e_b - r_s i_c - l_{\sigma c}\frac{di_c}{dt} - e_c}^{(+V_H)} \quad (5)$$

$$-V_H = \overbrace{r_s i_c + l_{\sigma c}\frac{di_c}{dt} + e_c - r_s i_a - l_{\sigma a}\frac{di_a}{dt} - e_a}^{(+V_H)} \quad (6)$$

where $+V_H$ is the H-Bridge DC Link voltage, r_s is the stator resistance per phase, and e_a is the back emf in phase a. The superscripts $\overbrace{\ }^{(+V_H)}$ denote that the measurement is made during the $+V_H$ test pulse.

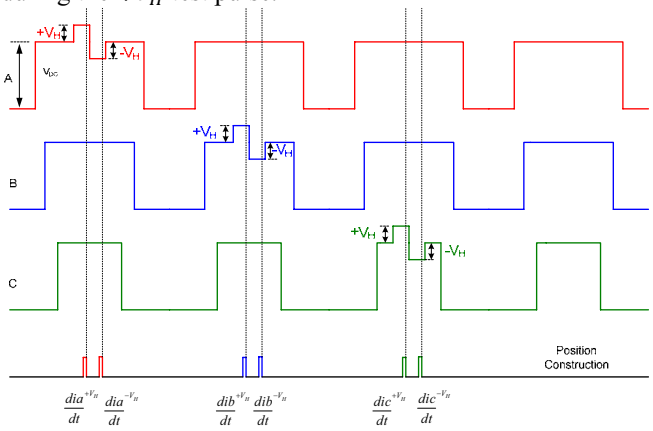

Fig 4: Switching pattern of the multilevel converter drive and the sequence for di/dt measurement and position construction

In a similar way, when H-Bridge A imposes the $-V_H$ test pulse the following equations can be derived:-

$$-V_H = \overbrace{r_s i_a + l_{\sigma a}\frac{di_a}{dt} + e_a - r_s i_b - l_{\sigma b}\frac{di_b}{dt} - e_b}^{(-V_H)} \quad (7)$$

$$0 = \overbrace{r_s i_b + l_{\sigma b}\frac{di_b}{dt} + e_b - r_s i_c - l_{\sigma c}\frac{di_c}{dt} - e_c}^{(-V_H)} \quad (8)$$

$$+V_H = \overbrace{r_s i_c + l_{\sigma c}\frac{di_c}{dt} + e_c - r_s i_a - l_{\sigma a}\frac{di_a}{dt} - e_a}^{(-V_H)} \quad (9)$$

Since the time between applying the $+V_H$ and $-V_H$ test vectors is very short, it can be assumed that:-

$$\overbrace{e_a}^{(+V_H)} = \overbrace{e_a}^{(-V_H)}\ ,\ \overbrace{e_b}^{(+V_H)} = \overbrace{e_b}^{(-V_H)}\ ,\ \overbrace{e_c}^{(+V_H)} = \overbrace{e_c}^{(-V_H)}$$

And also as the voltage across the stator resistance is small compared to the H-Bridge voltages $+V_H$ and $-V_H$ it can also be neglected. Subtracting equations (7),(8),(9) from equation (4),(5),(6) respectively yields:-

$$+2V_H = l_{\sigma a}\left(\frac{\overbrace{di_a}^{(+V_H)}}{dt} - \frac{\overbrace{di_a}^{(-V_H)}}{dt}\right) - l_{\sigma b}\left(\frac{\overbrace{di_b}^{(+V_H)}}{dt} - \frac{\overbrace{di_b}^{(-V_H)}}{dt}\right) \quad (10)$$

$$0 = l_{\sigma b}\left(\frac{\overbrace{di_b}^{(+V_H)}}{dt} - \frac{\overbrace{di_b}^{(-V_H)}}{dt}\right) - l_{\sigma c}\left(\frac{\overbrace{di_c}^{(+V_H)}}{dt} - \frac{\overbrace{di_c}^{(-V_H)}}{dt}\right) \quad (11)$$

$$\mathbf{-2V_H = l_{\sigma c}\left(\frac{\overbrace{di_c}^{(+V_H)}}{dt} - \frac{\overbrace{di_c}^{(-V_H)}}{dt}\right) - l_{\sigma a}\left(\frac{\overbrace{di_a}^{(+V_H)}}{dt} - \frac{\overbrace{di_a}^{(-V_H)}}{dt}\right)} \quad \mathbf{(12)}$$

From equations (10),(12) :-

$$\left(\frac{\overbrace{di_a}^{(+V_H)}}{dt} - \frac{\overbrace{di_a}^{(-V_H)}}{dt}\right) = \frac{+2V(l_{\sigma b} + l_{\sigma c})}{(l_{\sigma a}\, l_{\sigma b} + l_{\sigma b} l_{\sigma c} + l_{\sigma c} l_{\sigma a})} \quad (13)$$

And substituting $l_{\sigma a}\, l_{\sigma b} + l_{\sigma b} l_{\sigma c} + l_{\sigma c} l_{\sigma a}$ by $3L_0\left(1 - \left(\frac{\Delta L}{2L_0}\right)^2\right)$ yields:-

$$\left(\frac{\overbrace{di_a}^{(+V_H)}}{dt} - \frac{\overbrace{di_a}^{(-V_H)}}{dt}\right) = \frac{-2V(2L_0 - \Delta L cos(n_{an}\theta_{an}))}{3L_0\left(1 - \left(\frac{\Delta L}{2L_0}\right)^2\right)} \quad (14)$$

By defining the constant $g = \frac{3\left(1-\left(\frac{\Delta L}{2L_0}\right)^2\right)}{2V_H}$, the rotor position scalar for the a phase can then be defined as:-

$$\mathrm{P_a} = 2 + \mathrm{g}\left(\frac{\overbrace{di_a}^{(+V_H)}}{dt} - \frac{\overbrace{di_a}^{(-V_H)}}{dt}\right) \quad (15)$$

Repeating for phases b and c yields the following equations for position scalars $\mathrm{P_b}$, $\mathrm{P_c}$:-

$$\mathrm{P_b} = 2 + \mathrm{g}\left(\frac{\overbrace{di_b}^{(+V_H)}}{dt} - \frac{\overbrace{di_b}^{(-V_H)}}{dt}\right) \quad (16)$$

$$\mathrm{P_c} = 2 + \mathrm{g}\left(\frac{\overbrace{di_c}^{(+V_H)}}{dt} - \frac{\overbrace{di_c}^{(-V_H)}}{dt}\right) \quad (17)$$

The final form for the α and β components of the rotor slot position scalar will be :-

$$\mathrm{P_\alpha} = \mathrm{P_a} - \frac{1}{2}(\mathrm{P_b} + \mathrm{P_c}) \quad (18)$$

$$\mathrm{P_\beta} = \frac{\sqrt{3}}{2}(\mathrm{P_b} - \mathrm{P_c}) \quad (19)$$

The scalar position signals, $\mathrm{P_\alpha}$ and $\mathrm{P_\beta}$ are similar to resolver signals, and the rotor position can be extracted from them using suitable signal processing. They therefore require the

measurement of the motor line current derivative at specific instants of time, i.e. di/dt in response to specific test pulses.

5 Improvements to Current Distortion by using H-Bridge Converters

The optimum H-Bridge voltage that provides good position estimation quality and low current distortion was found by trial and error to be 150V. At this excitation voltage, the t_{min} is reduced from 25µs (required for both the standard 2 level INFORM method and the fundamental PWM method) to 20 µs. The improvement to current distortion obtained by using the new scheme can be measured by calculating the Total Harmonic Distortion (THD) of the motor line current when it is running in sensored mode at 30 rpm and under no load. For the following results Method 1 – time interval -1,0 - corresponds operation without any modifications to the PWM pattern (i.e. normal sensored vector control), Method 2 – time interval 0,2 – includes modifications to the PWM for operation with the proposed new multilevel scheme; Method 3 – time interval 2,4 - includes modifications to the PWM for operation with standard 2 level INFORM [1] and Method 4 – time interval 4,6 - includes modifications to the PWM for operation with standard 2 level fundamental PWM method [3]. The current waveforms obtained are shown in Fig 7. The current was measured using LeCroy CP150 current probes and LeCroy - WR 6050A oscilloscope, and was sampled at 10 MHz.

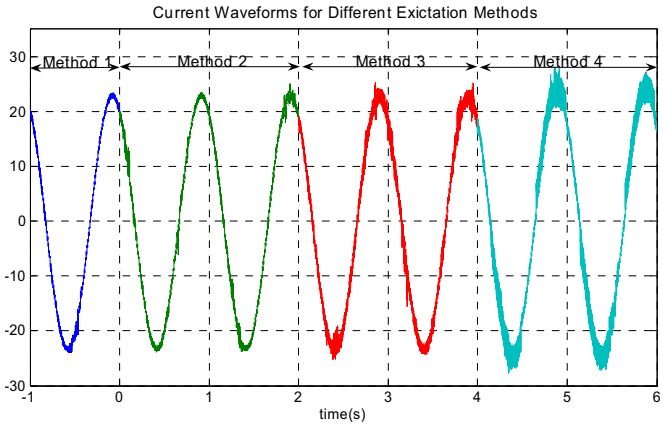

Fig 7: Current waveform for different excitation methods.

The THD values for the currents shown in Fig 7 are given in the Table 1 and Fig 8. It is clear from the current waveforms as well as from the THD calculations that a significant improvement is achieved using the new multilevel method. This improvement can be noticed also from the reduction in the audible noise when the new method is applied compared to that when the INFORM method and the Fundamental PWM method are used.

No load, 30 rpm, Sensored mode				
Excitation method	Method 1	Method 2	Method 3	Method 4
THD	1.92%	2.20%	6%	8.54%

Table1: THD for the different excitation methods.

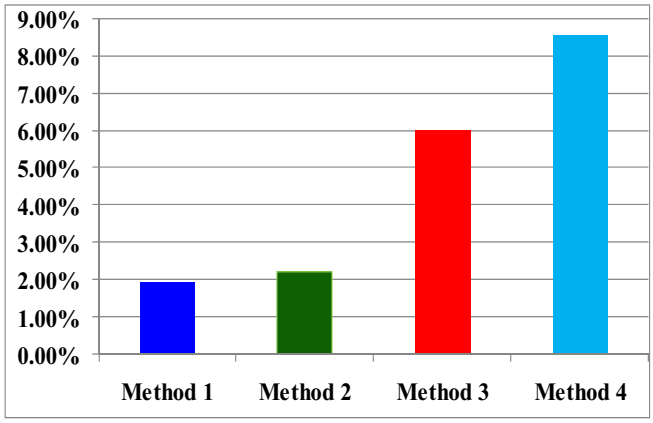

Fig 8: THD for the different excitation methods.

Although the proposed method is able to reduce the current distortion significantly, it will also reduce the Signal to Noise Ratio (SNR) of the di/dt signal measured and hence affect the quality of the position estimation. To overcome this problem, a novel current derivative sensor is used in this work. The new di/dt sensor improves the sensitivity up to 25 times over the old transformer-type di/dt sensor used in [3], and hence increases the SNR [10].

6 Rotor Position Estimation

The anisotropy caused by the rotor slotting was tracked using the proposed method ie measuring di/dt in response to the test vector sequence of Fig. 4. The position signals $P\alpha$ and $P\beta$ derived for the experimental system described in the previous section obtained using (18) and (19) are show in Fig. 9.

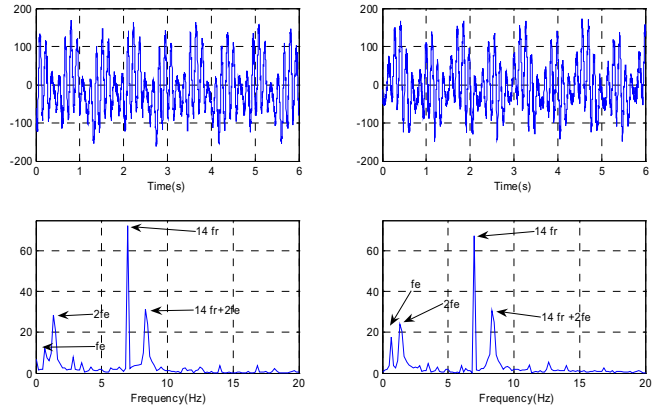

Fig 9 Top: α (left) and β (right) components of the estimated position signal at 15 rpm ,50% load. Bottom: Frequency spectrum of α (left) and β (right) components of the estimated position.

The rotor slotting saliency $(14\,f_r)$ is clear, but other disturbance harmonics are present which distort the position estimate. The $(2f_e)$ and (f_e) components are due to the saturation in the machine and the unbalance in the di/dt sensors respectively and the component $(14f_r + 2f_e)$ arises because the position signal $(14f_r)$ is modulated by saturation in the machine $(2f_e)$. The disturbance elemination method proposed in [11] is used to remove the $(2f_e)$ and (f_e) . This method assumes that these components will vary due to the

load conditions only, and is independent of the speed. The disturbance at $(14f_r + 2f_e)$ is removed by using the sideband filter in the rotating frame $14\theta_r + 2\theta_e$ proposed in [12] as shown in fig. 10.

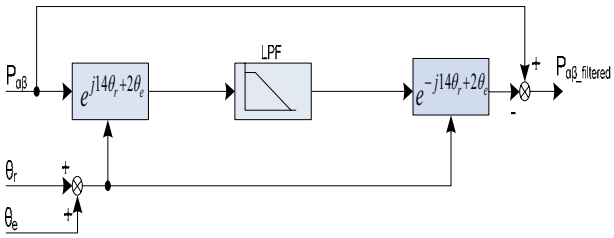

Fig 10: Schematic of the side band filter.

The position signals after filtering are shown in Fig. 11. It can be seen that the rotor slotting effect is now much stronger and is now suitable for rotor position tracking.

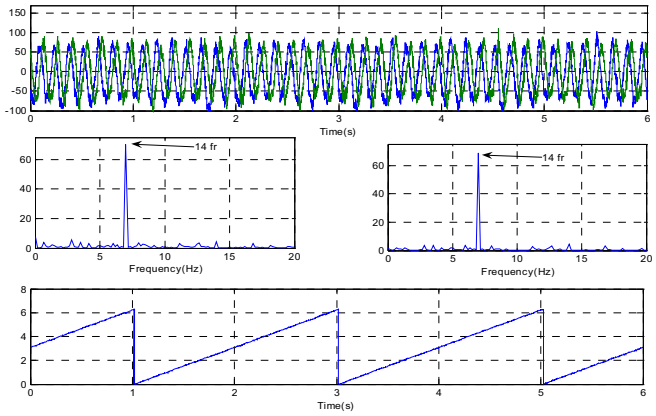

Fig 11: Top: filtered α and β component of the estimated position at 15 rpm ,50% load. Middle: FFT of α (left) and β (right) component of the estimated position. Bottom:- estimated rotor position.

The quality of the estimated position signal shown in the figure above is good enough to be used in a complete sensorless system as will be described in the next section.

7 Experimental Results for Sensorless Control

The proposed method has been implemented on an squirrel cage, star connected, 4 pole, 16kW, 50Hz induction motor with 28 semi-closed, non-skewed rotor slots. The switching frequency of the main Inverter was 5 kHz, and the H-Bridge DC link voltage used in the experiment was 150V. The width of the H-Bridge test vectors were 20 us and the rated current for the H-Bridges was 70% of the machine rated load and so the maximum safe load that can be applied to the machine is 50% of the rated load.

After filtering the raw position signals from the disturbances, the α and β component of this position signal is used with the mechanical observer described in [13]. The estimated rotor position and speed are then used for field orientation and speed feedback for a sensorless speed control system as shown in Fig 12.

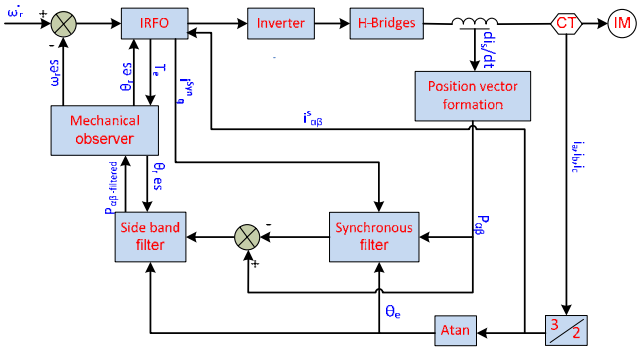

Fig 12: System setup of the sensorless speed control

Figures 13, 14, and 15 show the results of full sensorless speed control under no load and loaded conditions using the proposed method. In Fig 13 a speed step change from 450 to 0 back to 450 rpm at no load was demanded to show the method works over a wide speed range. The estimated speed and position seen in the figure proved that the system responded to the speed steps with good dynamic response and good steady state behaviour. In Fig 14 speed step changes between 12 and -12 rpm were applied to the system at no load, and the speed and position response of the system measured through the encoder for evaluation. The results show that the system can work very well at low speed as well as at high speed. Figure 15 shows speed step changes between 100 and 0 rpm with 50% load applied to the system. Again the speed measured from the encoder shows that the fully sensorless system has a very good speed response, even under load.

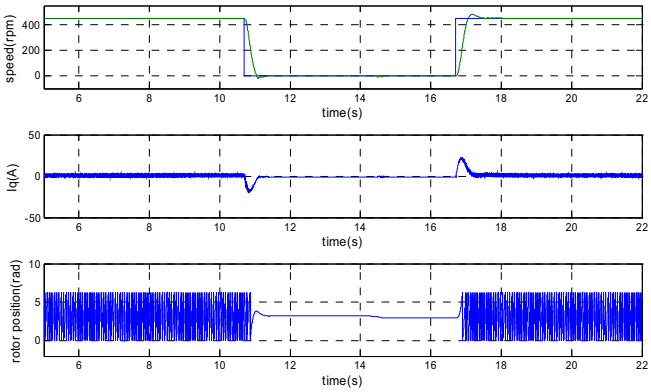

Fig 13 Fully sensorless speed control at no load using the proposed method. Top: reference speed (blue) and measured speed (green), Middle: Iq. Bottom: measured rotor position (blue) .

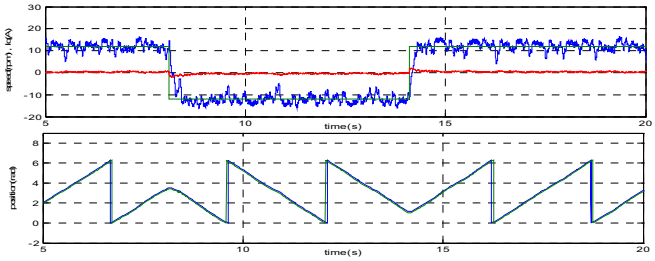

Fig 14: Fully sensorless speed control at no load using the proposed method. Top: reference speed (green) , measured

speed (blue), Iq(red). Bottom: measured rotor position (green) and estimated rotor position (blue)

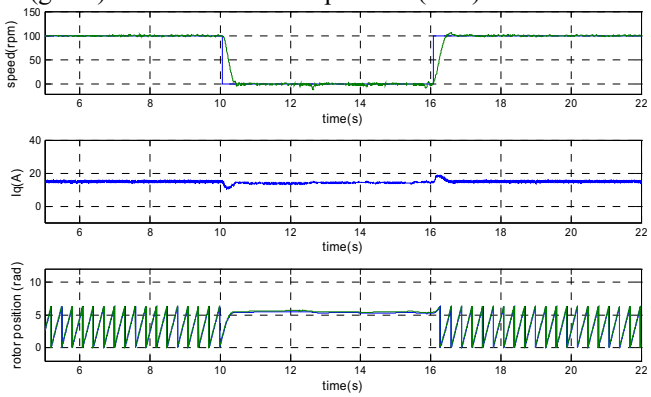

Fig 15: Fully sensorless speed control at 50% Load using the proposed method. Top: measured speed (blue). Bottom: Iq (blue), measured rotor position (green) and estimated rotor position (blue)

Fig 16 shows the system response to a load steps between 0 and 50% load. The motor took 0.5 seconds to recover.

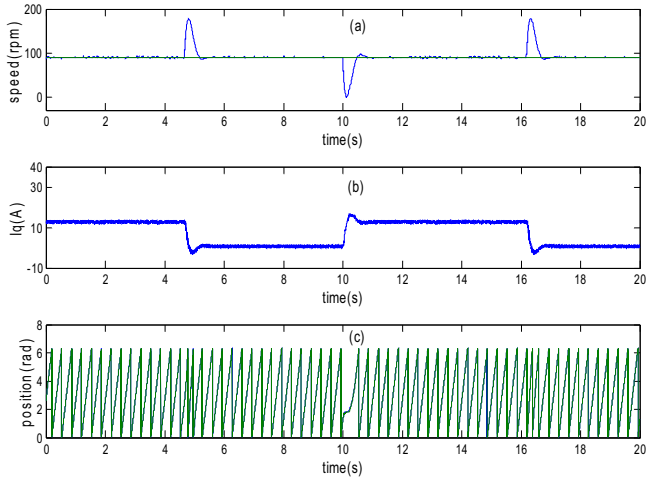

Fig 16: Load steps between 50% and 0 load using the proposed method (a) measured speed in blue, reference speed in green (b) Iq (c) measured rotor position in blue and estimated rotor position in green.

The results above show that the system can work successfully in full sensorless speed control mode.

8 Conclusion

This paper has outlined a new scheme for reducing the current distortion introduced into induction motor drives by low speed sensorless control techniques. The sensorless scheme used estimates the rotor position by using low voltage H-Bridges connected in series with a standard two level inverter to generate low voltage test vectors. By reducing the test vector size from 620V (standard DC link voltage for a 2 level inverter) to 150V (H Bridge DC link) the current ripple associated with the minimum active pulse width extension is reduced, although it will also have an effect on the di/dt measurement i.e decrease the signal to noise ratio (SNR). This challenge is overcome by using the new di/dt sensors introduced in [10]. Experimental results show that the new multilevel sensorless method achieves a significant improvement to the THD of the motor current, reducing it from 8.54% and 6% (2 level fundamental PWM method and the INFORM method respectively) to 2.2% when the new sensorless technique is used. The experimental results also demonstrate the correct control behaviour of the fully speed sensorless control at low and higher speeds at different load conditions.

The paper has demonstrated the viability of using additional H bridges for sensorless induction motor control. The cost of this approach will be prohibitive for low to medium power drives. However, high power induction motors are now being constructed using multi-level inverters, and therefore the techniques described here are very suitable to this class of motor drives.

References

[1] M. Schroedl. “Sensorless Control of AC Machines at Low Speed and Standstill Based on the INFORM Method”. IEEE IAS Annual Meeting, volume 4, pp. 270-277, (1996).

[2] J. Holtz, J. Juliet.”Sensorless Acquisition of the Rotor Position Angle of Induction Motors With Arbitrary Stator Windings”. IAS Annual Meeting, volume 2, pp.1675-1682, (2004).

[3] G.Qiang, G.M.Asher, M.Sumner.M, P.Makys. “Position Estimation of AC Machines at all Frequencies Using Only Space Vector PWM based Excitation”, 3rd IET International Conference , pp. 61-70, (2006).

[4]E.Robeischl, M.Schroedl. “Optimized INFORM Measurement Sequence for Sensorless PM Synchronous Motor Drives with Respect to Minimum Current Distortion.” IEEE Transactions on Industrial Applications, volume 40, pp.591-598,(2004).

[5] C. Staines, C.Caruana, G. M. Asher , M. Sumner. “Sensorless Control of Induction Machines at Zero and Low Frequency using Zero Sequence Currents”, IEEE Transaction on Industrial Electronics, volume 53, pp.195-206,(2006).

[6] A.Kempski, R.Smolenski , E.Kot. “Mitigation Techniques of Conducted EMI in Multilevel Inverter Drives“, IEEE Compatibility in Power Electronics, pp. 218 – 222, (2005).

[7] D-W. Kang,Y-H.Lee, B-S.Suh , C-H.Choi, D-S.Hyun. “An Improved Carrier-Based SVPWM Method Using Leg Voltage Redundancies in Generalized Cascaded Multilevel Inverter Topology”, IEEE Transactions on Power Electronics, volume 18, pp.180 – 187,(2003).

[8] M.D.Manjrekar, P.K.Steimer, T.A.Lipo,” Hybrid Multilevel Power Conversion System: A competitive Solution for High-Power Applications”, IEEE Transactions on Industry Applications, volume 36, pp 834–841, (2000)

[9] S.Kouro, R.Bernal, H.Miranda, C.A. Silva, J.Rodriguez, “High-Performance Torque and Flux Control for Multilevel Inverter Fed Induction Motors”, IEEE Transactions on Power Electronics, volume 22, pp 2116 – 2123,(2007).

[10] M.Tomasini , S.Bolognani, “Innovative control algorithms for electric drives – Time optimal current and torque control of IPM SM drives and experimental rig to test a rotor anisotropy-based sensorless vector control of IM drives”, PhD thesis, University of Padua, Italy, (2007).

[11] P.Makys, G.M.Asher, M.Sumner ,Q.Gao, J.Vittek. “A low Memory Disturbance Elimination Method for Sensorless Control of Induction Motor Drive Using Test Vector Injection” ,IECON 2006,pp.1071-1076 .

[12] J. Holtz,H. Pan, “Elimination of Saturation Effects in Sensorless Position Controlled Induction Motors”, IEEE Transaction in Industrial Application, volume 40, pp.623-631, (2000).

[13] R.D. Lorenz , K.W. Van Patten. “High-Resolution Velocity Estimation for All-Digital, ac Servo Drives” , IEEE transactions on industry applications, volume 27, pp.701 – 705, (1991).

[14] K.Saleh, G.M.Asher, M.Sumner, M.Tomasini, G.Qiang. “Low Speed Sensorless Control of an Induction Motor Fed by Multilevel Converter to Reduce Current Distortion”, EPE 2009 Sept 2009, Barcelona Spain.